Y. T. Chen

Institute of Energy and Environment,
Malaysia University of Science and Technology,
C901, Kelana Square, No. 17, Jln SS7/26,
Kelana Jaya, 47301 Petaling Jaya, Selangor,
Malaysia
email: ytchen@must.edu.my

A. Kribus

Dept. of Fluid Mechanics and Heat Transfer,
Faculty of Engineering, Tel Aviv University,
Tel Aviv 69978, Israel
email: kribus@yarkon.eng.tau.ac.il

B. H. Lim

email: bhlim@must.edu.my

C. S. Lim

email: cslim@must.edu.my

K. K. Chong

email: kkchong@must.edu.my

Institute of Energy and Environment, Malaysia
University of Science and Technology,
C901, Kelana Square, No. 17, Jln SS7/26,
Kelana Jaya, 47301 Petaling Jaya,
Selangor, Malaysia

J. Karni

Environmental Science and Energy Research
Department, Weizmann Institute of Science,
Rehovot 76100, Israel
email: Jacob.karni@weizmann.ac.il

R. Buck

email: reiner.buck@dlr.de

A. Pfahl

email: andreas.pfahl@dlr.de

Institute of Technical Thermodynamics,
German Aerospace Center (DLR)
Pfaffenwaldring 38-40,
Stuttgart 70569, Germany

T. P. Bligh

Department of Engineering,
University of Cambridge
Trumpington Street, Cambridge, CB2 1PZ,
United Kingdom
email: tpb@eng.cam.ac.uk

Comparison of Two Sun Tracking Methods in the Application of a Heliostat Field

The basic mathematics and structure of heliostat have remained unchanged for many decades. Following the challenge first made by Ries et al., the non-imaging focusing heliostat recently proposed by Chen et al. provides an alternative in the field of concentrated solar energy. This paper investigates the performance of a heliostat field composed of the newly proposed heliostats. In contrast to the dynamic curvature adjustment proposed in our previous work for a solar furnace, a fixed asymmetric curvature is used here with the spinning-elevation tracking method. This restriction is intended to equalize the manufacture cost of the new heliostat with that of traditional heliostats with azimuth-elevation tracking and spherical curvature. Fixing the curvature results in only partial aberration correction, compared to full correction using the dynamic adjustment of curvature. Nevertheless, the case studies presented in this paper show that the new heliostat design can reduce the receiver spillage loss by 10–30%, and provide a much more uniform performance without large variations with time of day.
[DOI: 10.1115/1.1634583]

1 Introduction

It has been a long tradition since the beginning of application of heliostats that heliostat mirror alignment approximates spherical curvature, and sun tracking is performed with azimuth-elevation axes. The conventional heliostat suffers from strong astigmatic aberration whenever the reflection is off-axis, which is most of the time in practical situations. The aberration increases the sun's image size on the target considerably relative to the on-axis situation, leading to a significant spillage loss, a reduction in the average flux on the receiver, and a reduction in receiver efficiency. Several authors attempted to tackle this problem. In their detailed theoretical study on the traditional heliostat, Igel and Hughes [1] realized that the amount of aberration depends on the incidence angle as

measured in the tangential plane, defined by the sun, the center of the heliostat, and the target. They pointed out that the image size could be reduced if the heliostat can be constructed with asymmetric curvature, but this requires that the heliostat be aligned with the tangential plane rather than just pointing at the target (the distinction between alignment and pointing is explained in [2]). They proposed to rotate the heliostat frame about the normal of the center facet, in addition to the azimuth and elevation motions, to achieve this alignment. This is mechanically cumbersome and too expensive to be practical.

Ries [3] and Zaibel et al. [4] made another proposal to use a target aligned mount method for sun tracking. In this method, the sagittal and tangential directions are fixed with respect to the heliostat frame. The aberration can then be corrected by using a non-symmetric heliostat with two different radii of curvature. They noted that the correction is different for each time, and computed the fixed asymmetric curvature that would provide the best annual average correction. Chen et al. [5,6] derived the sun tracking formula for the spinning-elevation tracking mount, where the spinning axis points towards the target and keeps the heliostat normal within the tangential plane, and the elevation axis rotates the heliostat normal within the tangential plane. They proposed a heliostat with a dynamically adjusted geometry that has the ability to make a full aberration correction. Unlike the conventional imaging heliostat design where a fixed geometry approximating a spherical surface is used, the new heliostat has no specific geometry. It is composed of a number of smaller movable facet mirrors, which can be maneuvered to make the first-order aberration correction. The new design was therefore named "non-imaging focusing heliostat".

The shape of the non-imaging focusing heliostat is similar to the shape of non-symmetric geometry proposed by Ries et al. [3,4], having two different radii of curvature along the row and column directions. However, this is only true when the distance between the target and heliostat is large relative to the dimension of the heliostat. In the case of small distance, the required curvature of the heliostat surface varies along the tangential direction. The orientation of the facets in different rows is therefore asymmetric with respect to the center of the heliostat. In the solar furnace demonstration [6], two separate driving units were used to control the movements of the facets in the lower and upper parts of the heliostat, due to this asymmetry.

Even a conventional heliostat using azimuth-elevation tracking could make a full aberration correction, if its facets were permitted to move during the tracking. However, this is not feasible since each individual facet requires a specific motion with two degrees of freedom, leading to complex control and prohibitive cost. The spinning-elevation tracking method, on the other hand, provides the only mode to link the movements of all the facets using a small number of motors, and thus reduce the number of controls to the minimum.

The application of non-imaging focusing heliostats in a heliostat field, e.g., in a solar power plant, requires a significant emphasis on cost reduction since the heliostat cost is a major factor in the overall plant cost-effectiveness. A fixed geometry of the heliostat is therefore preferred relative to the dynamic facet alignment. In this paper, we will discuss the comparison of two heliostat field systems, both employing heliostats with a fixed geometry. The facets in the conventional heliostat field are aligned according to the traditional spherical curvature to achieve the required focal distance. The facets in the non-imaging heliostat field have an additional degree of freedom, and provide both the needed focal distance and a partial aberration correction. This additional degree of freedom will be used to optimize the flux distribution on the target.

2 Comparison Method

2.1 Comparison Criterion. Zaibel et al. [4] used the area of the illuminated region on the target plane (often called the
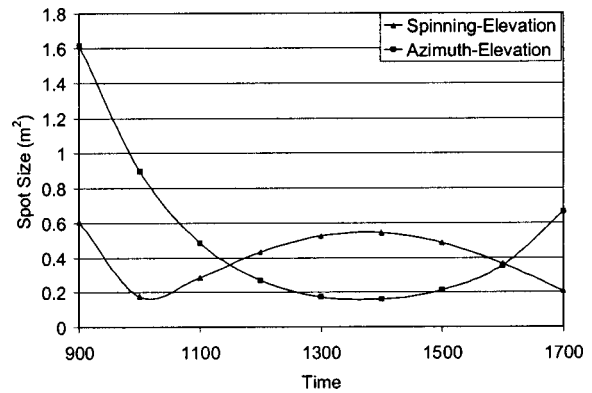

Fig. 1 Spot size comparison between the spinning-elevation and azimuth-elevation tracking methods for June 21st. The target angle is 41.8 deg, facing angle is 10 deg to the south and the latitude is North 43 deg. Heliostat area is 25 m² and the slant range is 30 m.

"spot") as a criterion to compare the performance of traditional and aberration corrected heliostats. This type of comparison is shown in Fig. 1. However, the comparison of the spot area is not sufficient for practical design. This comparison does not reflect the effect of spot's shape, which in many cases is the dominant factor in determining the receiver spillage loss and intercept efficiency. For traditional heliostats, the spot shape is distorted into an approximately elliptical shape with non-uniform flux most of the time. The spillage loss can therefore be larger than the value that would be estimated based on spot area alone. An aberration corrected heliostat, on the other hand, will produce a nearly circular spot shape most of the time. Therefore, an appropriate comparison of the performance of the two types of heliostats requires accounting for the spot shape.

The size and shape of the spot on the receiver's plane are determined by two main factors: the disc effect (spreading of the radiation within the solid angle subtended by the sun), and the astigmatic aberration. The calculation methods are all well known [1]. The disc effect depends on the slant range but not on heliostat design, and is therefore the same for all types of heliostats. The astigmatic aberration can be divided into two components: aberration of individual facets, and the residual aberration spread due to imperfect canting [7]. The facet-level aberration is relatively small in practical cases where the heliostat facets are small relative to the slant range. The residual aberration can be small if the facets are continuously adjusted to provide a dynamic astigmatic correction [5] that follows the variations in incidence angle. When the facets are preset, i.e., given a fixed orientation, then this aberration is zero at one particular incidence angle matching the preset, and larger at other angles [7]. Therefore, the residual aberration is the main source of differences in the performance of the different heliostats.

Two methods are employed in this study to present the comparison between heliostat types. The image-spread method [7] provides a qualitative presentation of the residual astigmatic aberration. The intercept points on the target plane for central rays from each heliostat facet are plotted; with ideal canting, they should all intersect at the center of the target. The spread of the intercept points is a measure of the deviation from perfect canting, and is correlated with spillage losses for an aperture of a given size. The characteristic curve method [8] provides a more quantitative and comprehensive information for comparison. The intercept efficiency is plotted vs. the average flux concentration, with the aperture radius serving as the parameter that changes along the curve. This characteristic curve shows the two performance indicators, efficiency and concentration, simultaneously for any receiver size.

The flux distribution on the target and the spillage losses corresponding to the two heliostat designs were computed using a computer simulation program. The intercept at the target plane of the central ray from each facet was computed using ray tracing. The program calculated the size and shape of the spot for each individual facet in the heliostat. The flux within the spot created by an individual facet was assumed to be uniform. The overall flux distribution created by the heliostat is a superposition of the distributions of the individual mirrors. The intercepted power is then given by an integration of the flux distribution within a given aperture on the target plane.

Due to the high degree of complexity and the large number of geometric parameters, it is difficult to generalize the comparison results. Therefore, we have studied some specific cases as illustration. The design shown here for the heliostat geometry and field layout is one choice, and readers may apply the method described here to other geometric designs according to their own application.

2.2 Sun Tracking Algorithms. The mathematical expressions for the two sun tracking methods were previously published [5], and are presented here briefly for completeness. The relevant tracking angles and the distinct characteristics of the two he-

Table 1 Parameters for comparison of heliostats

Heliostat size	5 m×5 m
Size of facet	1 m×1 m
Tower height	20 m
Facing angle	135°
Latitude	43° North
Facet focusing distance	46 m
Target distance (slant range)	28.6 m

liostats are schematically shown in Fig. 2, and the geometry of the heliostat relative to the tower is illustrated in Fig. 3.

For azimuth-elevation tracking, the heliostat azimuth angle A_A and the heliostat elevation angle θ_A are as follows:

$$A_A = \text{ArcSin}\left(\frac{\text{Cos } \lambda \text{ Sin } \phi + \text{Cos } \alpha \text{ Sin } A}{2 \text{ Cos } \theta \text{ Cos } \theta_A} \right) \tag{1}$$

$$\theta_A = \text{ArcSin}\left(\frac{-\text{Sin } \lambda + \text{Sin } \alpha}{2 \text{ Cos } \theta} \right) \tag{2}$$

For spinning-elevation tracking, the heliostat spin angle ρ_S and the heliostat elevation angle θ_S are as follows:

$$\rho_S = \text{ArcSin}\left(\frac{-\text{Cos } \delta \text{ Cos } \omega \text{ Sin } \phi \text{ Sin } \Phi + \text{Cos } \delta \text{ Sin } \omega \text{ Cos } \phi + \text{Sin } \delta \text{ Sin } \phi \text{ Cos } \Phi}{\text{Cos}(\pi/2 - 2\theta)} \right) \tag{3}$$

$$\theta_S = \theta \tag{4}$$

In the above, θ is the incidence angle:

$$\theta = 0.5 \text{ ArcCos}(-\text{Sin } \lambda \text{ Sin } \alpha + \text{Cos } \lambda \text{ Sin } \phi \text{ Cos } \alpha \text{ Sin } A$$
$$+ \text{Cos } \lambda \text{ Cos } \phi \text{ Cos } \alpha \text{ Cos} A) \tag{5}$$

α is the solar altitude angle:

$$\alpha = \text{ArcSin}(\text{Sin } \delta \text{ Sin } \Phi + \text{Cos } \delta \text{ Cos } \omega \text{ Cos } \Phi) \tag{6}$$

A is the solar azimuth angle (if Sin $\omega > 0$ then $A = 2\pi - A$):

$$A = \text{ArcCos}\left(\frac{\text{Sin } \delta \text{ Cos } \Phi - \text{Cos } \delta \text{ Cos } \omega \text{ Sin } \Phi}{\text{Cos } \alpha} \right) \tag{7}$$

λ is the target angle; ϕ is the facing angle; δ is the declination angle; Φ is the latitude; and ω is the hour angle.

3 Comparison for a Single Heliostat

The parameters used for the comparison of the performance of single heliostats are given in Table 1. The conventional heliostat facet alignment is assumed to approximate a fixed spherical geometry (on-axis canting), while the spinning-elevation heliostat used a fixed facet geometry according to the non-imaging alignment procedure [5]. The presetting incidence angles are 0 degree for conventional heliostat and 31.4 degree for spinning-elevation heliostat. The location of the heliostat relative to the tower corresponds to position 7 in the field shown in Fig. 4.

The disc effect and aberration effect for individual mirrors are insensitive to the choice of tracking axes and the canting of the heliostat, and are therefore the same for the two heliostats. Therefore, the performance difference between the two heliostats is mainly due to the residual aberration. This effect is clearly seen by comparing the residual image spread. The image spread distributions at different times are shown in Fig. 5. The results show two important distinctions. First, if we compare the results at a given
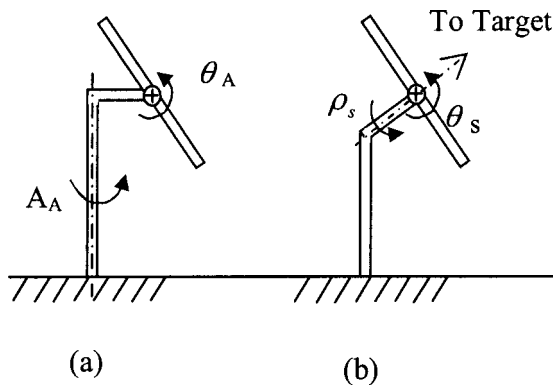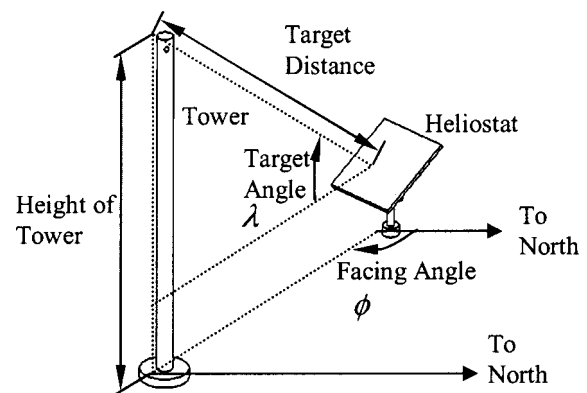

Fig. 2 The schematic diagram shows the difference between the two kinds of sun tracking methods: (a) azimuth-elevation; (b) spinning-elevation.

Fig. 3 The definitions of geometric parameters used in the comparison of heliostats
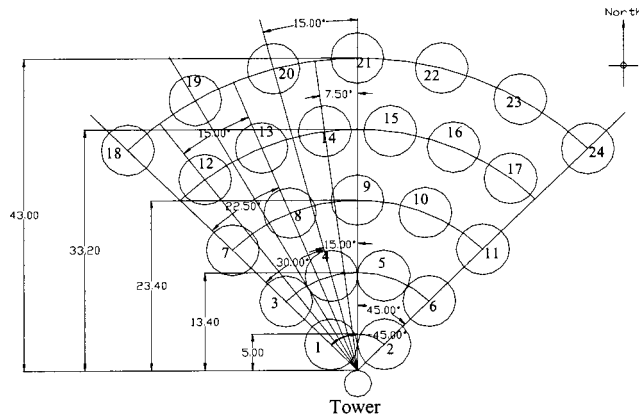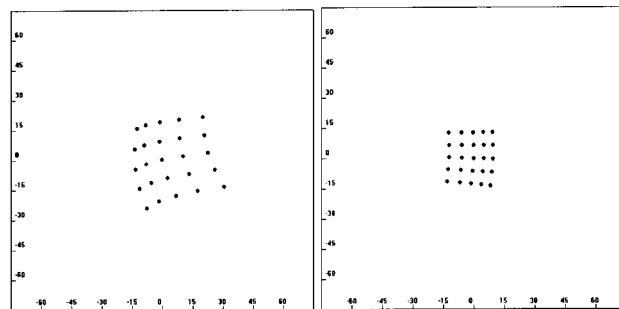
Fig. 4 The layout shows the heliostat field used for comparison between the two types of heliostat design. The dimensions shown are in meters. The tower height is 20 m. The specifications for each heliostat are given in Table 1.
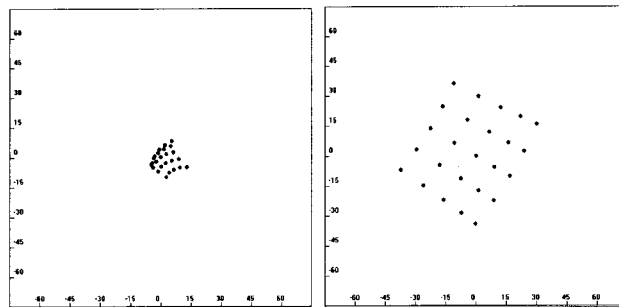
time, we find that the space distribution of the spread in the traditional heliostat is uneven, while in the non-imaging heliostat it is nearly uniform. This flux non-uniformity created by the traditional heliostat could be related to "hot spots" that often occur in existing solar tower plants, causing damage to receivers. A solar plant with the new non-imaging focusing heliostats should provide a more uniform flux distribution and alleviate this problem. A second observation is that the time variation of the spread of the traditional heliostat is much larger than that of non-imaging focusing heliostat.

To quantify the effect of these differences on the performance of a receiver, the intercept efficiency and the average concentration at the receiver aperture, for a wide range of receiver radii, were computed for the flux distributions created by the two heliostats using the data obtained in Fig. 5. The results for several times during the day of June 21 are shown in Fig. 6. The temporal variability is clearly observed in these results. For example, if we keep the receiver intercept efficiency fixed at 90%, the variation in concentration at the receiver during the day is larger for the traditional heliostat by a factor of 2.5.
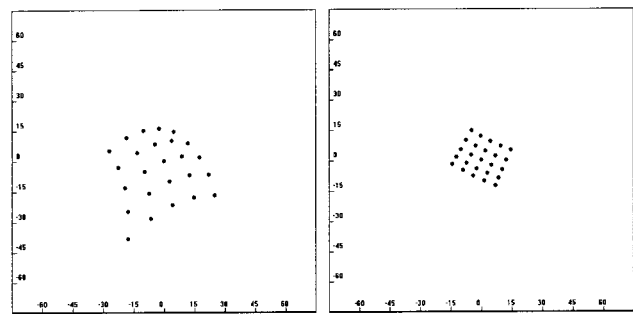
Figure 7 shows the maximum spillage loss for the two types of heliostat as a function of receiver aperture radius. The maximum
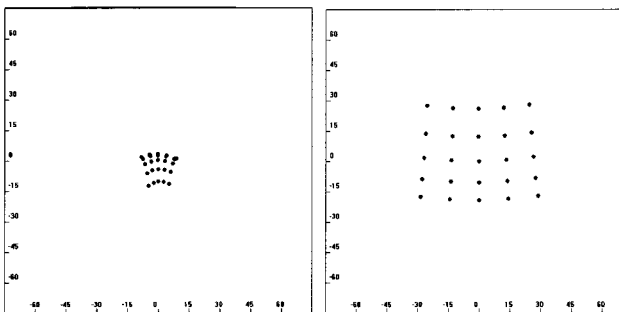

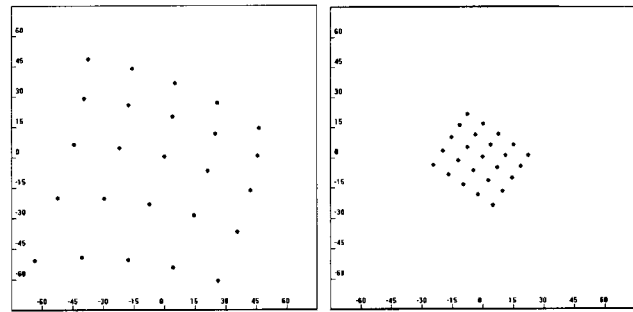
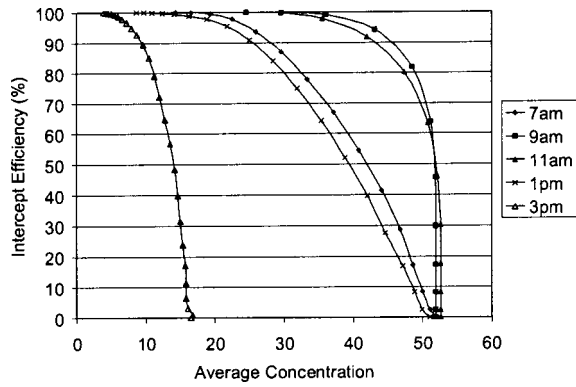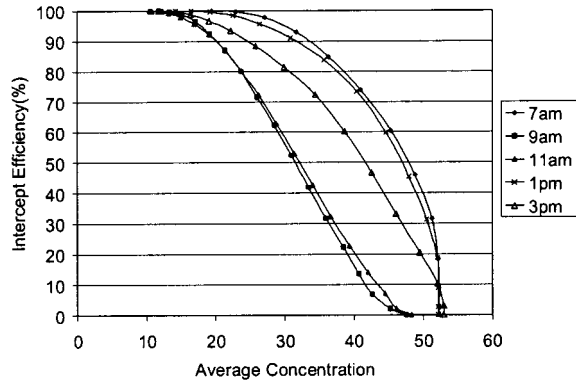**Fig. 5 The comparison of image spread for heliostat 7 at different times on June 21. The dimensions shown are in centimeters. Each point represents the intersection on the target plane of a central ray from an individual facet. Left side: traditional heliostat; right side: non-imaging focusing heliostat. (*a*) 7 am. (*b*) 9 am. (*c*) 11 am. (*d*) 1 pm. (*e*) 3 pm.**

(a)

(b)

Fig. 6 The characteristic curves for heliostat 7 at different times during June 21. (*a*) Traditional heliostat. (*b*) Non-imaging focusing heliostat.

spillage is significantly higher for the traditional heliostat. For an aperture size in the range of 1–2 m, the new heliostat may provide about 30% reduction in spillage loss relative to the traditional heliostat.

4 Comparison for a Group of Heliostats

4.1 "Smoothing" Procedure Using Different off-Axis Presetting for a Group of Heliostats. In the previous section we have shown that flux distribution created by a single non-imaging
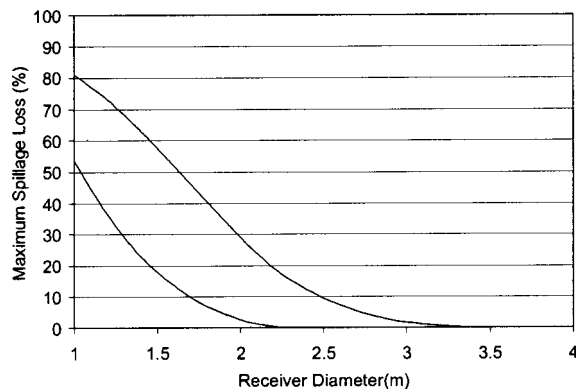

Fig. 7 The yearly maximum spillage loss is shown as a function of the receiver diameter. Upper curve: traditional heliostat. Lower curve: new heliostat.
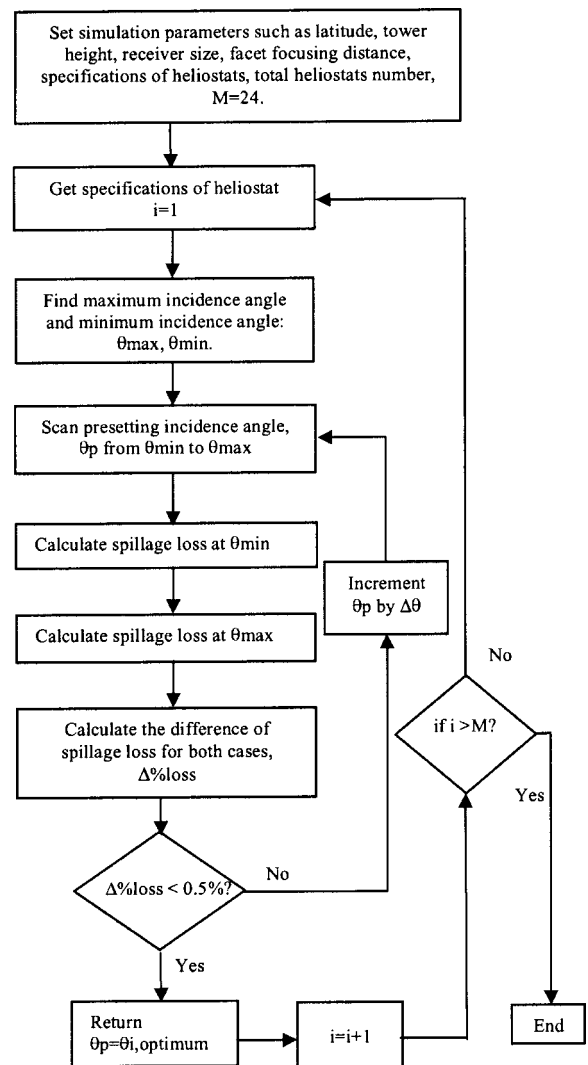

Fig. 8 The flow chart of smoothing process

focusing heliostat is much more stable than that created by a conventional heliostat, showing smaller variations during the day. The time variation of the received solar flux during the daily operation of a heliostat field can be improved even further by utilizing an important feature of the non-imaging focusing heliostat. The traditional heliostat can only use on-axis presetting (canting), which is only suitable for reflection at normal incidence. The new heliostat may use off-axis presetting, which can refer to any incidence angle. This provides an additional degree of freedom that enables optimization of the field performance. Figure 1 shows that the spot area for a non-imaging focusing heliostat with fixed facet geometry varies with incidence angle, and reaches a minimum when the incidence angle is equal to the preset incidence angle used in fixing the facet orientation. We can choose to preset each heliostat within the group such that its minimum spot area will occur at a different time (incidence angle is a function of time) relative to other members of the group. This choice will average out the received solar flux for a daily operation. A proper selection of the individual preset times can then lead to a flux distribution that does not vary much during the day.

Figure 8 gives the procedures of the smoothing process. By providing a receiver size, scanning process is executed to find the optimum presetting angle (θ_p) where the spillage loss at maximum incidence angle (θ_{max}) is equal to that of minimum incidence angle (θ_{min}) for the particular heliostat. After the presetting
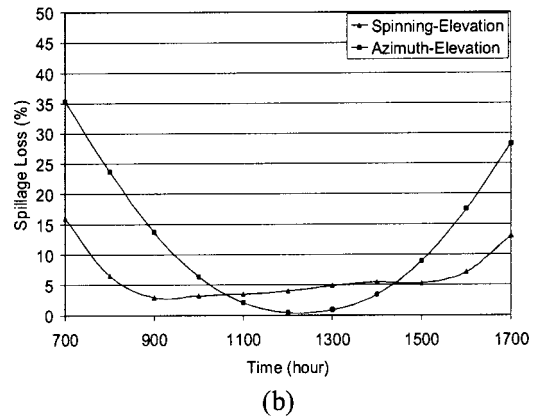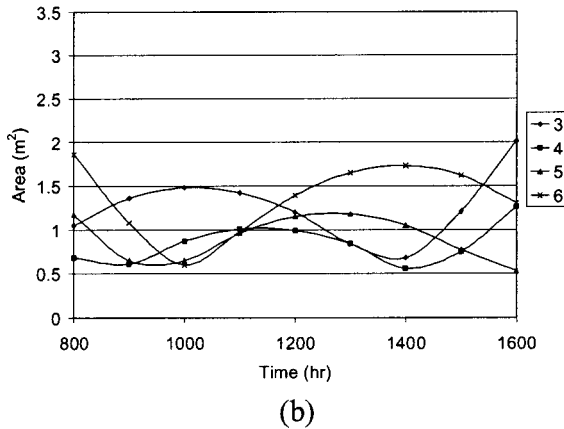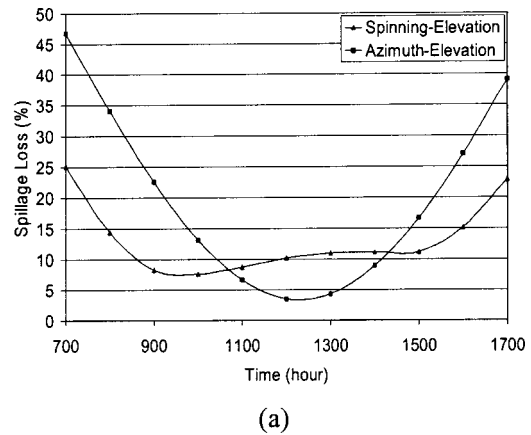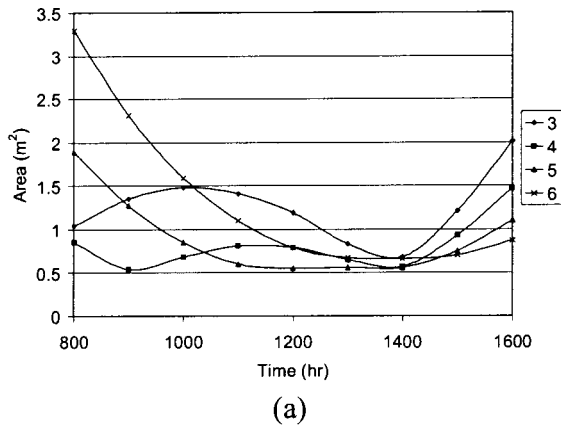
(a)

(b)

Fig. 9 The smoothing procedure is demonstrated for heliostats 3, 4, 5 and 6 during Nov. 21 (*a*) Presetting time for all four heliostats are the same i.e. 2 pm, 21st Jan. (*b*) The presetting time for each heliostat is optimized to produce a relatively uniform distribution during daily operation.

angle for the first heliostat is found, the process is repeated for the other heliostats, i.e., 2nd, 3rd, 4th, ... Mth. According the flow chart, the process can be done manually or by a computer program. In the present case study, because the involved number of the heliostat is not that many (a total of 24), the process was carried out manually.

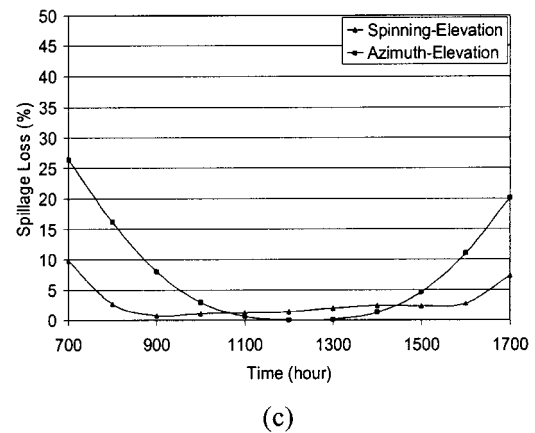Figure 9 compares the time variation of the spot area between

Fig. 10 The best and worst characteristic curves for both sun-tracking methods are plotted. The characteristic curves for all other times are within the two limits.

(a)

(b)

(c)

Fig. 11 The time variation of spillage loss for the entire field diameter is plotted for both sun-tracking methods during June 21. (*a*) Receiver aperture diameter is 1 m. (*b*) Aperture diameter 1.2 m. (*c*) Aperture diameter 1.4 m.

the cases of a single preset and an optimized set of individual presets. Only four heliostats are shown for clarity. In the case of a single preset time for all heliostats which was preset on 2PM of 21 January, the variation of solar flux with time is high. In the second case with individual preset incidence angles, the off-axis preset was done at 2PM of 21 January for heliostat 3, at 9AM of 21 January for heliostat 4, at 9:50 AM of 21 January for heliostat 5, and at 10:30 AM of 21 January for heliostat respectively, the time variations of each heliostat is seen to compensate for the variations of the others, resulting in a much smaller overall variation. This unique degree of freedom provides a new way to smooth the daily variation of received solar power. Other methods employed
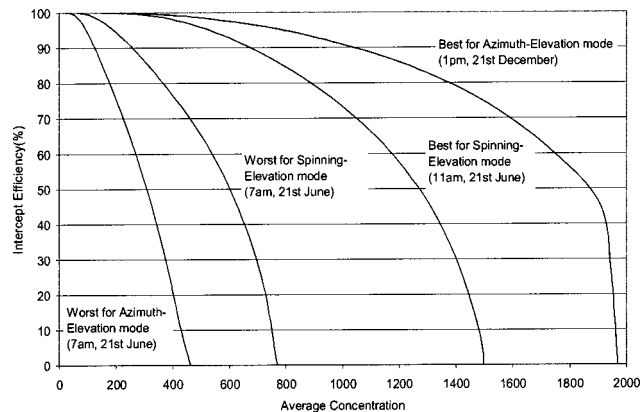
today to compensate for daily flux variations are quite complex and require active control of variable aim points for individual heliostats [9,10].

4.2 Performance of a Heliostat Field. A small field of 24 heliostats, as shown in Fig. 4, serves to demonstrate the difference between the traditional and new heliostat designs. An overview of the annual variability in field performance is shown in Fig. 10. The characteristic curves, intercept efficiency vs. concentration, are shown for the limiting cases of best and worst performance during the year. The best and worst times for the field composed of traditional heliostat are 1 PM on December 21 and 7 AM on June 21, respectively. The best and worst times for the field with the new heliostat field are 11 AM on June 21 and 7 AM on June 21, respectively. For most values of intercept efficiency, the new method brings only half of the variation in concentration than that of the traditional method. It is true that the using of traditional heliostat sometimes can reach high concentration, but this is achieved at the expense of low concentration at the other times. This high variability is undesirable in the design and operation of solar power plants, and a stable and uniform level of concentration is preferable.

The spillage loss during June 21 for three specific receivers with aperture diameters of 1 m, 1.2 m and 1.4 m is shown in Fig. 11. The field using the new heliostat the receiving efficiency can remain at a low loss level for most of the day. Even at other times, 10–30% reduction in spillage loss is achievable.

5 Conclusions

We have compared the performance of two tracking methods at the level of a single heliostat and a heliostat field. The two types of heliostat designs are the new non-imaging focusing heliostat using off-axis preset geometry, and the traditional spherical heliostat with on-axis preset (canting). The comparison of a single heliostat showed that the new design offers much less variation in the image spread, leading to a more uniform flux both in space and in time. The comparison of a heliostat field showed again a significant reduction in time variability of the incident flux, and a significant advantage of the new heliostat design in reduction of spillage loss.

The increased uniformity of the incidence flux, both in spatial distribution and in temporal variations, is beneficial for receiver performance. Variations of the flux in space and time can be detrimental, especially when the receiver may be damaged when the flux level or local temperature exceed some threshold. The new heliostat design has a significant effect of smoothing the spatial flux distribution and the time variations, and therefore can make a significant contribution towards alleviating these problems.

The test case studied here includes a small North field. In larger surround fields with a significant number of heliostats in the other sides of the tower, the advantage of the new design can be even larger. Heliostats located East, West and South of the tower operate usually at higher incidence angles relative to Northern heliostats. The performance of conventional heliostats is poor under these conditions, but the new heliostat design can be optimized using a preset suitable for its range of incidence angles.

The most impressive feature of the new heliostat design is that the higher performance is achieved possibly without extra cost. The geometric design of the heliostat is different, but contains precisely the same elements. The required manufacturing, assembly and alignment procedures are therefore similar. Even if switching from manufacturing of conventional heliostats, the only needed investment is the initial mechanical redesign and some modification of the tracking software. This combination of better performance and the same cost, achieved with aberration-corrected heliostats, can lead to a more effective and attractive use of solar energy.

References

[1] Igel, E. A., and Hughes, R. L., 1979, "Optical Analysis of Solar Facility Heliostat," Sol. Energy, **22**, pp. 283–295.

[2] Kribus, A., and Ries, H., "LiMoNAED: a Limited Motion, Non-Shading, Asymmetric, Ecliptic-Tracking Dish," Sol. Energy **73**, pp. 337–344.

[3] Ries, H., and Schubnell, M., 1990, "The Optics of a Two-Stage Solar Furnace," Solar Energy Materials, **21**, pp. 213–217.

[4] Zaibel, R., Dagan, E., Karni, J., and Ries, H., 1995, "An Astigmatic Corrected Target-Aligned Heliostat for High Concentration," Solar Energy Materials and Solar Cells, **37**, pp. 191–202.

[5] Chen, Y. T., Chong, K. K., Bligh, T. P., Chen, L. C., Jasmy, Y., Kannan, K. S., Lim, B. H., Lim, C. S., Alias, M. A., Noriah, B., Omar, A., Sahar, S., Shk. Abd. Rezan, S. A. H., Tam, C. M., and Tan, K. K., 2001, "Non Imaging Focusing Heliostat," Sol. Energy, **71**, pp. 155–164.

[6] Chen, Y. T., Chong, K. K., Lim, C. S., Lim, B. H., Tan, K. K., Omar, A., Bligh, T. P., Tan, B. K., and Ghazally, I., 2002, "Report of the First Prototype of Non-Imaging Focusing Heliostat and Its Application in High Temperature Solar Furnace," Sol. Energy, **72**, pp. 531–544.

[7] Chen, Y. T., Chong, K. K., Lim, B. H., and Lim, C. S., 2003, "Study of Residual Aberration for Non-Imaging Focusing Heliostat," Solar Energy Materials and Solar Cells, In Press.

[8] Spirkl, W., Timinger, A., Ries, H., Kribus, A., and Muschaweck, J., 1998, "Non-Axisymmetric Reflectors Concentrating Radiation From an Asymmetric Heliostat Field Onto a Circular Absorber," Sol. Energy, **63**, pp. 23–30.

[9] Vant-Hull, L. L., and Pitman, C. L., 1990, "*Static and Dynamic Response of a Heliostat Field to Flux Density Limitation on a Central Receiver*," J. T. Beard and M. A. Ebadian (Editors), *Solar Engineering*, pp. 31–38.

[10] Valverde, A., and Weinrebe, G., 1996, "Implementation of an Automatic Aim-Point Strategy for a Volumetric Receiver in the PSA CESA-1 Heliostat Field," *8 Int. Symp. Solar Thermal Concentrating Technologies*, Becker, M., and Böhmer, M., Eds., Köln, C. F. Müller, **2**, pp. 1047–1065.